Inorganic Chemistry

Article

pubs.acs.org/IC

Solid-State ^{29}Si NMR and Neutron-Diffraction Studies of $Sr_{0.7}K_{0.3}SiO_{2.85}$ Oxide Ion Conductors

Jungu Xu,[†] Xiaoming Wang,[‡] Hui Fu,[‡] Craig M. Brown,[§,∥] Xiping Jing,[‡] Fuhui Liao,[‡] Fengqi Lu,[⊥] Xiaohui Li,[⊥] Xiaojun Kuang,*[,⊥,†] and Mingmei Wu*[,†]

[†]MOE Key Laboratory of Bioinorganic and Synthetic Chemistry, State Key Laboratory of Optoelectronic Materials and Technologies, School of Chemistry and Chemical Engineering, Sun Yat-Sen University, Guangzhou 510275, P. R. China

[‡]Beijing National Laboratory for Molecular Sciences, The State Key Laboratory of Rare Earth Materials Chemistry and Applications, College of Chemistry and Molecular Engineering, Peking University, Beijing 100871, P. R. China

[§]NIST Center for Neutron Research, National Institute of Standards and Technology, Gaithersburg, Maryland 20899, United States

[∥]Department of Chemical and Biomolecular Engineering, University of Delaware, Newark, Delaware 19716, United States

[⊥]Guangxi Ministry-Province Jointly-Constructed Cultivation Base for State Key Laboratory of Processing for Nonferrous Metal and Featured Materials, MOE Key Laboratory of New Processing Technology for Nonferrous Metals and Materials, College of Materials Science and Engineering, Guilin University of Technology, Guilin 541004 P. R. China

Supporting Information

ABSTRACT: K/Na-doped $SrSiO_3$-based oxide ion conductors were recently reported as promising candidates for low-temperature solid-oxide fuel cells. $Sr_{0.7}K_{0.3}SiO_{2.85}$, close to the solid-solution limit of $Sr_{1-x}K_xSiO_{3-0.5x}$, was characterized by solid-state ^{29}Si NMR spectroscopy and neutron powder diffraction (NPD). Differing with the average structure containing the vacancies stabilized within the isolated Si_3O_9 tetrahedral rings derived from the NPD study, the ^{29}Si NMR data provides new insight into the local defect structure in $Sr_{0.7}K_{0.3}SiO_{2.85}$. The Q^1-linked tetrahedral Si signal in the ^{29}Si NMR data suggests that the Si_3O_9 tetrahedral rings in the K-doped $SrSiO_3$ materials were broken, forming Si_3O_8 chains. The Si_3O_8 chains can be stabilized by either bonding with the oxygen atoms of the absorbed lattice water molecules, leading to the Q^1-linked tetrahedral Si, or sharing oxygen atoms with neighboring Si_3O_9 units, which is consistent with the Q^3-linked tetrahedral Si signal detected in the ^{29}Si NMR spectra.

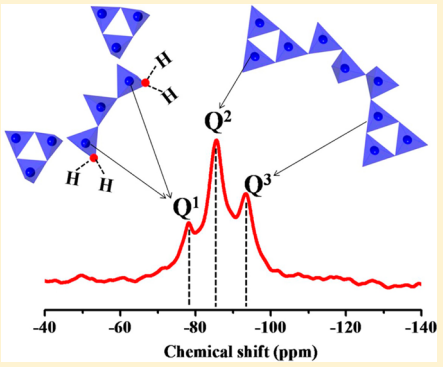

1. INTRODUCTION

Solid-oxide fuel cells (SOFCs) have particular advantages over other types of fuel cells because of their modularity and fuel flexibility allowing the use of a range of fuels from high-purity H_2 to readily available hydrocarbons.[1,2] For SOFCs, the electrolyte transporting the oxide ion from cathode to anode plays a key role in determining the optimum operating temperature. The conventional and commercialized electrolyte yttria stabilized zirconia (YSZ)[3] requires high operating temperatures (800−1000 °C) to achieve sufficient oxide ion conductivity, which increases the cost and exacerbates instability issues from both the mechanical and chemical compatibilities between the components in the SOFCs. There is therefore considerable interest in developing alternative electrolytes with oxide ion conductivity exceeding 10^{-2} S/cm at low temperatures between 500 and 700 °C.[4] Materials showing high oxide ion conductivity and displaying new combinations of charge carrier and structural prototype are particularly attractive,[5−7] such as the tetrahedral structures displaying high oxygen interstitial or vacancy mobility without necessary constraint of the high lattice symmetries.[8−11] Typical interstitial oxide ion conducting tetrahedral structure examples include $Ln_{10-x}(MO_4)_6O_{3-1.5x}$ (Ln is a rare earth element; M = Si, Ge) apatites[9,12] and $La_{1+x}A_{1-x}Ga_3O_{7+0.5x}$ (A = Sr, Ca) melilites.[8,13] In these structures, tetrahedrons that are available to increase their coordination number with terminal oxygen atoms are favorable geometries for deformation and rotations, which are proven to be key factors for stabilizing and transporting the oxygen interstitials.[8] On the other hand, in these tetrahedral networks oxygen vacancy defects are not created straightforwardly but can be accommodated via corner-sharing with the neighboring tetrahedron, which maintains four-coordinate geometry, as observed in the isolated tetrahedral $La_{1-x}Ba_{1+x}GaO_{4-0.5x}$.[14]

Recently Goodenough et al. reported new oxide ion conductors of monoclinic Na/K-doped $SrMO_3$ (M = Si, Ge), which were proposed to accommodate mobile oxygen vacancies in the isolated corner-shared 3-fold cyclical tetrahedral trimer M_3O_9 (the structure of $SrSiO_3$ is given in Figure 1).[15,16] These isolated M_3O_9 units (Figure 1b,c) lying within the *ab* planes form tetrahedral layers that are separated from each other by

Received: April 15, 2014
Published: June 6, 2014

   dx.doi.org/10.1021/ic500891j | Inorg. Chem. 2014, 53, 6962−6968

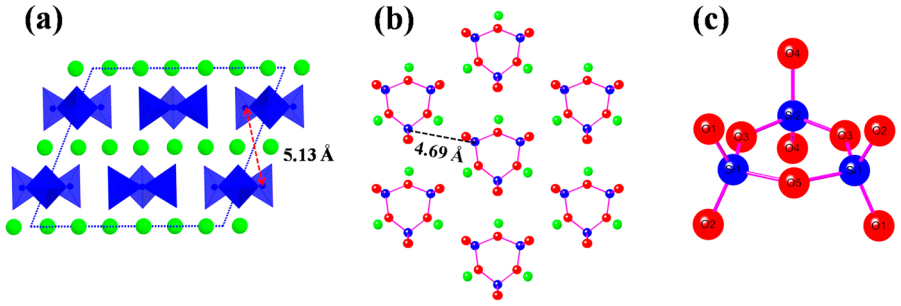

Figure 1. Structure of $SrSiO_3$. (a) View along the *b*-axis. (b) The Si_3O_9 ring arrangement within the tetrahedral layer. (c) A corner-sharing cyclical Si_3O_9 unit with 3-fold ring. The red, green, and blue spheres and tetrahedra denote O, Sr, and Si atoms and SiO_4 tedtrahedra, respectively. The shortest inter-ring Si−Si distances within intertetrahedral layers (a) and intratetrahedral layers (b) are labeled.

close-packed layers of large Sr^{2+} ions along the *c*-axis (Figure 1a). Goodenough et al. proposed that the steric hindrance by the large Sr^{2+} and Na^+ or K^+ cation layers between the isolated cyclical M_3O_9 layers did not permit corner-sharing of the neighboring M_3O_9 units to accommodate terminal oxygen vacancies. They also were concerned about the possibility of distortions of the M_3O_9 units to introduce interstitial sites for sharing corners with the neighboring cyclical units. More recently Goodenough et al. provided further evidence of the stabilization of oxygen vacancies in $M_3O_{9-\delta}$ rings by steric hindrance in the Na/K-doped $SrMO_3$ (M = Si, Ge) from neutron-diffraction data,[17] which suggested no interstitial oxygen atoms for corner-sharing between the $M_3O_{9-\delta}$ rings in the structures and revealed a preferred distribution of oxygen vacancies on the bridging oxygen sites over the terminal oxygen sites at room temperature and more random dispersion over all the oxygen sites at high temperature.

In general, diffraction techniques probe the average structure but not the local structure, for which solid-state nuclear magnetic resonance (NMR) is a powerful tool.[12,18−20] In silicate materials, solid-state ^{29}Si NMR, as an effective way of studying the SiO_4 linkage geometries,[21−26] was applied in studying the coordination environment of Si in the defect structure induced by the presence of interstitial oxygen in apatite-type oxide ion conductors with isolated SiO_4 tetrahedra.[19] In this work, we investigated the defect structure of $Sr_{0.7}K_{0.3}SiO_{2.85}$, which is close to the solid solution limit of $Sr_{1-x}K_xSiO_{3-0.5x}$ and is expected to possess the highest level of oxygen defects among the $Sr_{1-x}K_xSiO_{3-0.5x}$ series, by solid-state ^{29}Si NMR spectra and neutron powder diffraction (NPD) measurements. From the ^{29}Si NMR data, we propose a mechanism for stabilization of oxygen vacancies in the $SrSiO_3$ tetrahedral structure, involving breaking the Si_3O_9 rings to form Si_3O_8 chains, which are stabilized by coordinating with the absorbed lattice water molecules or linking with the neighboring Si_3O_9 rings, in great contrast to average structure containing the oxygen vacancies stabilized within the isolated $Si_3O_{9-\delta}$ rings from the NPD data.[27]

2. EXPERIMENTAL SECTION

Starting materials $SrCO_3$ (>99%), K_2CO_3 (>99%), and SiO_2 (>99%) according to the nominal compositions $Sr_{1-x}K_xSiO_{3-0.5x}$ (x = 0.1, 0.2, 0.3, and 0.4) were weighed and mixed in ethanol in an agate mortar, followed by calcination at 900 °C for 12 h in crucibles covered with lids. The powders were ground and refired at 1150 °C for 15 h to get final products of $Sr_{1-x}K_xSiO_{3-0.5}$. Approximately 10 g of $Sr_{0.7}K_{0.3}SiO_{2.85}$ powder was made according to this procedure for the NPD experiment. The parent $SrSiO_3$ material was prepared by being fired at 1150 °C for 15 h and 1250 °C for further 20 h.

The phase compositions were examined by powder X-ray diffraction (XRD) using a Bruker D8 ADVANCE powder diffractometer with Cu Kα radiation. Constant-wavelength NPD data of $Sr_{0.7}K_{0.3}SiO_{2.85}$ was collected at ambient temperature on the BT1 diffractometer at the National Institute of Standards and Technology (NIST). The sample was sealed under helium in a vanadium cell and was measured using the Cu(311) monochromator with a 90° takeoff angle and in-pile collimation of 60 min of arc (λ = 1.540 30 Å). Data was collected over the 2θ range of 3°−168° with a step size of 0.05°. All diffraction data analyses were performed using Topas Academic software.[28] The composition of $Sr_{0.7}K_{0.3}SiO_{2.85}$ was examined by X-ray energy dispersive spectroscopy (EDS) performed on a FEI Quanta 400 Thermal FE Environment scanning electron microscope. The sample was coated with gold as a thin conducting layer prior to the EDS elementary analysis. Selected-area electron diffraction (SAED) was performed on a JEOL JEM-2100F field-emission transmission electron microscopy (TEM) with an accelerating voltage of 200 kV.

Solid-state NMR spectra were measured on a Bruker AVANCE III 400 MHz WB spectrometer operating at 79.51 MHz for ^{29}Si. Single pulse magic angle spinning (MAS) NMR experiments were carried out at a MAS of 10.0 kHz using zirconia rotors of 4 mm in diameter. The ^{29}Si $\pi/2$ pulse was 6.0 μs, and the relaxation delay was 300 s. Thermogravimetric analysis (TGA) was performed using a TA Instruments TGA Q500. The temperature was ramped to 800 °C at a heating rate of 10 °C/min with a nitrogen flow during the TGA experiments. Fourier transform infrared spectroscopy measurement was performed at 4000−400 cm^{-1} using a Nicolet Thermo Nexus 470 instrument on samples pressed with KBr. (Certain commercial suppliers are identified in this Paper to foster understanding. Such identification does not imply recommendation or endorsement by the National Institute of Standards and Technology, nor does it imply that the materials or equipment identified are necessarily the best available for the purpose.)

3. RESULTS

Neutron Powder Diffraction Analysis of $Sr_{0.7}K_{0.3}SiO_{2.85}$. The room-temperature XRD patterns of $Sr_{0.7}K_{0.3}SiO_{2.85}$ and the parent $SrSiO_3$ are shown in Figure 2, displaying that both of the materials formed single phase. In comparison with the K-doped compositions, the parent $SrSiO_3$ material required higher temperature to remove the Sr_2SiO_4 and SiO_2 impurities to achieve the singe phase. Consistent with the results reported by Goodenough et al.,[16] the solid-solution limit of $Sr_{1-x}K_xSiO_{3-0.5x}$ was found only to be extended to x = 0.3, above which, such as x = 0.4 in this work, an impurity of K_2SiO_3 was present in the samples. EDS elementary analysis on the composition $Sr_{0.7}K_{0.3}SiO_{2.85}$ (x = 0.3) gave cationic ratio $Sr_{0.67}K_{0.33}Si$, as shown in Figure 3, agreeing well with the nominal composition and indicating that the potassium content in the materials was not significantly altered by potassium volatilization in this study.

dx.doi.org/10.1021/ic500891j | Inorg. Chem. 2014, 53, 6962−6968

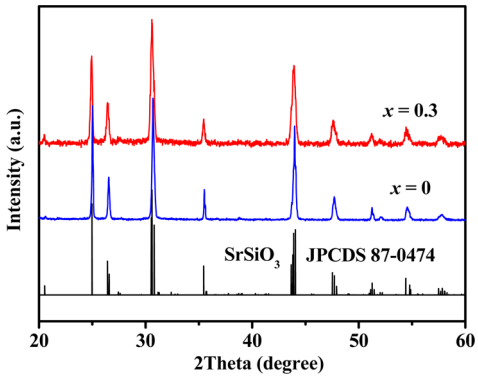

Figure 2. Room-temperature XRD patterns of $Sr_{1-x}K_xSiO_{3-0.5x}$ (x = 0 and 0.3). Spectrum in black shows expected peak positions and intensities for $SrSiO_3$ from JPCDS 87−0474.

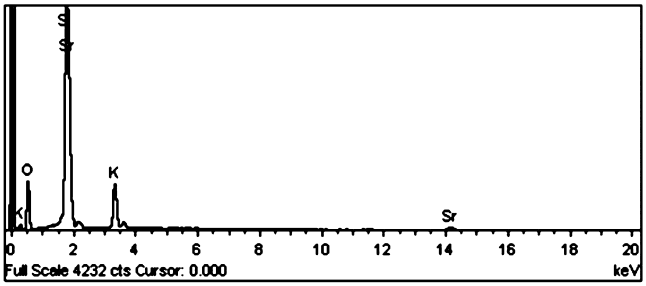

Figure 3. EDS spectrum of $Sr_{0.7}K_{0.3}SiO_{2.85}$. The cationic ratio of Sr/K/Si from EDS is about $Sr_{0.67}K_{0.33}Si$.

Prior to the neutron-diffraction measurement, electron diffraction (ED) patterns were collected on $Sr_{0.7}K_{0.3}SiO_{2.85}$, as shown in Figure 4, which confirmed the monoclinic unit cell of $a \approx 12.3$ Å, $b \approx 7.2$ Å, $c \approx 10.9$ Å, and $\beta \approx 111.6°$ within space group $C2/c$ or its subgroup Cc.

Rietveld refinement was performed on the room-temperature NPD data of the $Sr_{0.7}K_{0.3}SiO_{2.85}$ sample based on the structural model in $C2/c$ of parent $SrSiO_3$ reported by Nishi et al.,[29] which contains two Sr sites (8f for Sr1/K1 and 4c for Sr2/K2), two Si sites (8f for Si1 and 4e for Si2), four 8f (O1−O4), and one 4e (O5) oxygen sites. The occupancies on the Sr/K and oxygen sites were refined subject to the charge neutrality constraint. The refinement converged to reliability factors $R_{wp} \approx 4.2\%$ and $R_B \approx 1.6\%$ with a refined composition $Sr_{0.74(2)}K_{0.26(2)}SiO_{2.87(2)}$ close to the nominal composition. A preference distribution of oxygen vacancies on the bridging oxygen sites (O3 and O5 in Figure 1c) over the terminal oxygen sites (O1, O2, and O4 in Figure 1c) was obtained from the refinement, which is consistent with the results that were reported by Goodenough et al. for the compositions of $Sr_{1-x}Na_xSi_1O_{3-0.5x}$ (x = 0.2 and 0.4) and $Sr_{0.8}K_{0.2}Ge_{1-y}Si_yO_{2.9}$ (y = 0, 0.5).[17] The final refined structural parameters of $Sr_{0.7}K_{0.3}SiO_{2.85}$ obtained from the Rietveld refinement of the NPD data are given in Table 1, and the bond lengths are given in Table 2. The Rietveld plot of NPD data for $Sr_{0.7}K_{0.3}SiO_{2.85}$ is shown in Figure 5.

Solid-State ^{29}Si NMR Data. Consistent with the observation of Goodenough et al., the K-doped materials here are hygroscopic at room temperature. The existence of the OH^- group in the samples was confirmed by the infrared spectrum, which displays the characteristic vibration bands of OH^- at 3443 cm^{-1} (stretching) and 1625 cm^{-1} (bending). The

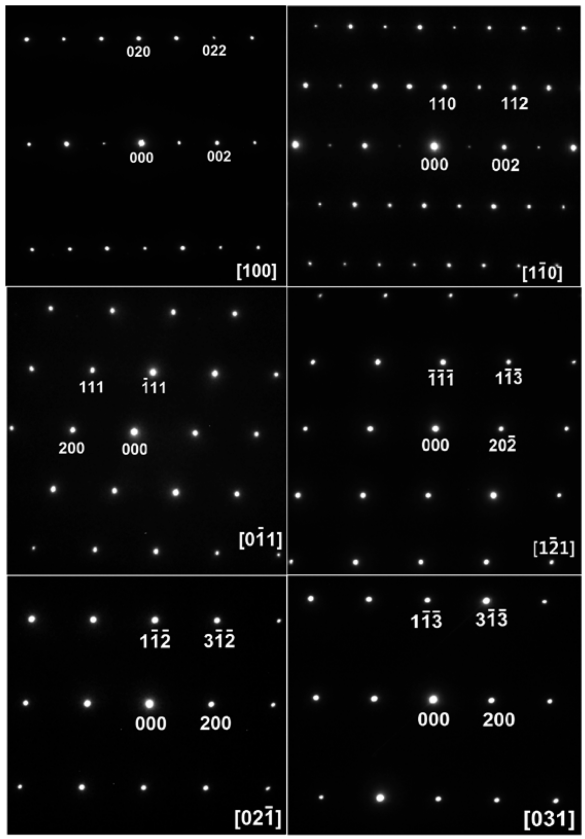

Figure 4. [100], [1$\bar{1}$0], [0$\bar{1}$1], [1$\bar{2}$1], [02$\bar{1}$], and [031] projections of ED patterns of $Sr_{0.7}K_{0.3}SiO_{2.85}$.

Table 1. Final Refined Structural Parameters of $Sr_{0.7}K_{0.3}SiO_{2.85}$[a]

atoms	occupancy	x	y	z	B_{iso} (Å^2)
Sr1(8f)	0.74(2)	0.0863(3)	0.2419(3)	0.4998(4)	0.02(1)
K1(8f)	0.26(2)	0.0863(3)	0.2419(3)	0.4998(4)	0.02(1)
Sr2(4c)	0.73(2)	0.25	0.25	0	0.16(3)
K2(4c)	0.27(2)	0.25	0.25	0	0.16(3)
Si1(8f)	1	0.1248(4)	0.4582(6)	0.2445(4)	0.78(3)
Si2(4e)	1	0	0.833(1)	0.25	1.3(1)
O1(8f)	0.977(7)	0.1279(3)	0.4115(5)	0.1060(3)	0.72(3)
O2(8f)	0.962(7)	0.2226(3)	0.4078(6)	0.3854(3)	0.72(5)
O3(8f)	0.929(8)	0.1069(3)	0.6875(5)	0.2488(3)	0.62(4)
O4(8f)	0.975(7)	0.0485(3)	0.9371(5)	0.3898(3)	0.99(6)
O5(4e)	0.919(1)	0	0.3685(7)	0.25	0.54(5)

[a] a = 12.3403(3) Å, b = 7.1495(1) Å, c = 10.8904(2) Å, β = 111.598(2)°, V = 893.38(4) Å^3, Z = 12 with space group $C2/c$; R_{wp} = 4.2%, R_p = 3.1%, R_B = 1.6%.

absorbed water molecules might enter into the oxygen vacancies, which could in turn affect the ^{29}Si NMR chemical shift of the materials. Under consideration of the influence of absorbed water on the ^{29}Si NMR data, three single-phase $Sr_{0.7}K_{0.3}SiO_{2.85}$ samples were prepared for the ^{29}Si NMR data collection. One $Sr_{0.7}K_{0.3}SiO_{2.85}$ sample was exposed to air at room temperature for 30 d, and the up-taken water content in this material determined by TGA data (Figure 6) is about 10.5 wt %. This sample is labeled as "hydrated $Sr_{0.7}K_{0.3}SiO_{2.85}$." To remove the absorbed water from the material, the hydrated $Sr_{0.7}K_{0.3}SiO_{2.85}$ sample was dried at 400 °C for 4 h, which gave a "dehydrated $Sr_{0.7}K_{0.3}SiO_{2.85}$" sample. The dehydration appa-

dx.doi.org/10.1021/ic500891j | Inorg. Chem. 2014, 53, 6962−6968

Table 2. Interatomic Distances and Bond Angles

bond	distance (Å)	bond	angle (deg)
Sr1/K1−O1(× 1)	2.747(4)	$Si1O_4$ tetrahedron	
Sr1/K1−O1(× 1)	2.703(4)	O1−Si1−O2(× 1)	126.8(3)
Sr1/K1−O2(× 1)	2.707(6)	O1−Si1−O3(× 1)	106.8(3)
Sr1/K1−O2(× 1)	2.469(4)	O1−Si1−O5(× 1)	107.5(3)
Sr1/K1−O3(× 1)	2.677(5)	O2−Si1−O3(× 1)	104.8(3)
Sr1/K1−O4(× 1)	2.448(4)	O2−Si1−O5(× 1)	104.8(3)
Sr1/K1−O4(× 1)	2.707(5)	O3−Si1−O5(× 1)	104.0(3)
Sr1/K1−O5(× 1)	2.687(4)		
Sr2/K2−O1(× 2)	2.493(4)	$Si2O_4$ tetrahedron	
Sr2/K2−O2(× 2)	2.711(4)	O4−Si2−O4(× 1)	124.7(1)
Sr2/K2−O3(× 2)	2.692(2)	O4−Si2−O3(× 2)	107.4(1)
Sr2/K2−O4(× 2)	2.686(3)	O4−Si2−O3(× 2)	105.9(1)
		O3−Si2−O3(× 1)	103.5(1)
$Si1O_4$ tetrahedron			
Si1−O1(× 1)	1.559(6)		
Si1−O2(× 1)	1.605(5)		
Si1−O3(× 1)	1.657(6)		
Si1−O5(× 1)	1.689(5)		
$Si2O_4$ tetrahedron			
Si2−O3(× 2)	1.686(6)		
Si2−O4(× 2)	1.598(5)		

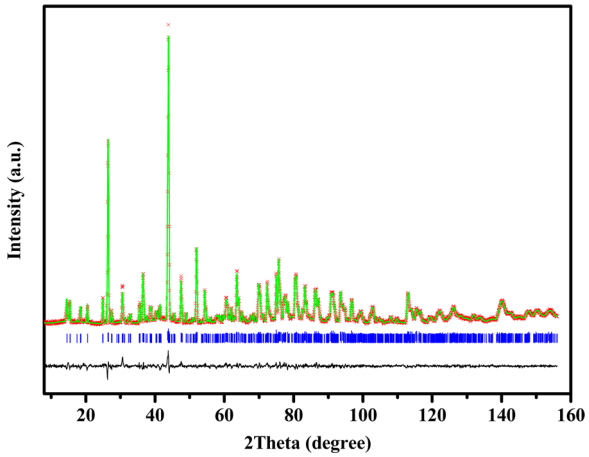

Figure 5. Rietveld refinement of NPD data for $Sr_{0.7}K_{0.3}SiO_{2.85}$. Experimental data are given as red crosses, the calculated profile is given by the green line, and the difference is given as the black curve underneath. Blue ticks indicate Bragg reflection positions.

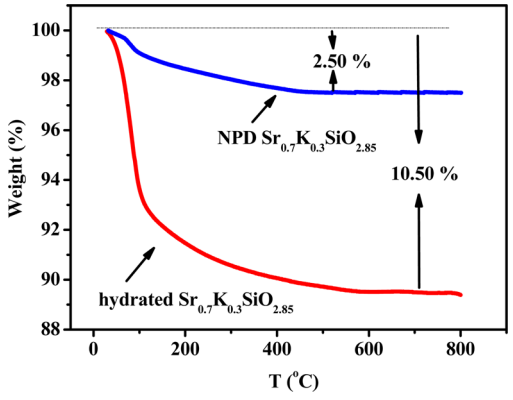

Figure 6. TGA data of $Sr_{0.7}K_{0.3}SiO_{2.85}$ samples.

rently reduced the cell volume to 892.34(1) from 894.53(2) $Å^3$ for the hydrated sample, and the cell volume for the dehydrated sample $Sr_{0.7}K_{0.3}SiO_{2.85}$ is even smaller than that for the parent $SrSiO_3$ material (893.67(1) $Å^3$) in spite of substitution of large K^+ cation for the smaller Sr^{2+}. This implies that oxygen deficiency is a predominate factor on modifying the cell volume of the K-doped $SrSiO_3$ over the K^+ substitution, in addition to the hydration in the K-doped samples. The as-prepared $Sr_{0.7}K_{0.3}SiO_{2.85}$ sample for the NPD data collection was additionally used for the NMR experiment; it is referred to as "NPD $Sr_{0.7}K_{0.3}SiO_{2.85}$." The solid-state ^{29}Si NMR spectra were collected on these three $Sr_{0.7}K_{0.3}SiO_{2.85}$ samples with the parent $SrSiO_3$ sample for comparison, and the results are shown in Figure 7.

The ^{29}Si NMR chemical shifts in solid silicates mainly depend on the degree of condensation of the silicon−oxygen tetrahedra. Increasing anion condensation, from a single to a double tetrahedra, and further to chains, layers, and finally to

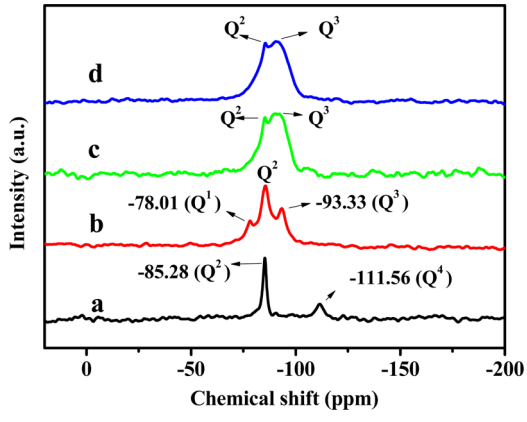

Figure 7. ^{29}Si NMR spectra of (a) $SrSiO_3$, (b) hydrated $Sr_{0.7}K_{0.3}SiO_{2.85}$, (c) dehydrated $Sr_{0.7}K_{0.3}SiO_{2.85}$, and (d) NPD $Sr_{0.7}K_{0.3}SiO_{2.85}$ samples. The chemical shift positions for the Q^1-, Q^2-, and Q^3-linked tetrahedral ^{29}Si signals are labeled.

dx.doi.org/10.1021/ic500891j | Inorg. Chem. 2014, 53, 6962−6968

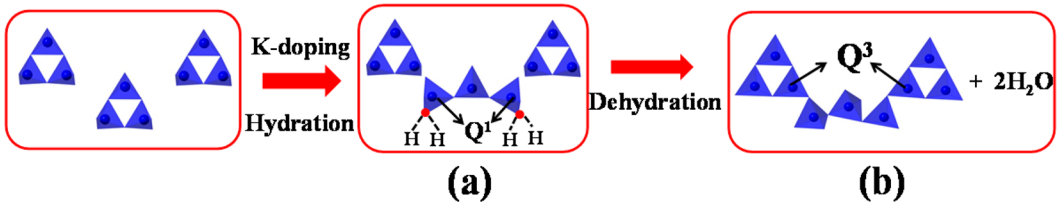

Figure 8. Schematic representations of possible local defect structures: (a) breaking of a $Si_3O_{9-\delta}$ ring forming a Si_3O_8 chain, where the terminal Si centers are stabilized by bonding with the oxygen atoms in the lattice water molecules; (b) linkage of a Si_3O_8 chain with two neighboring Si_3O_9 rings.

three-dimensional linked frameworks, leads to increasing ^{29}Si shielding.[25] The range of ^{29}Si chemical shifts in silicates varies from −60 ppm to −120 ppm for monosilicates (Q^0 ≈ from −68 to −76 ppm), disilicates and chain end groups (Q^1 ≈ from −76 to −82 ppm), middle groups in chains (Q^2 ≈ from −82 to −88 ppm), chain branching sites (Q^3 ≈ from −88 to −98 ppm), and the three-dimensional cross-linked framework (Q^4 ≈ from −98 to −129 ppm) according to an ascending sequence.[21,25] These typical ^{29}Si NMR chemical shifts allow discernment of the linkages of SiO_4 tetrahedra in the structures. As shown in the spectrum of the undoped $SrSiO_3$ (Figure 7a), the sharp peak around −85.28 ppm corresponds to the well-established Q^2-linked tetrahedral Si in the 3-fold cyclical Si_3O_9. The weak peak around −111.56 ppm is ascribed to the Q^4-linked tetrahedral Si, which may be attributed to the small amount of unreacted SiO_2 below the detection limit of XRD. The hydrated $Sr_{0.7}K_{0.3}SiO_{2.85}$ displays well-resolved three peaks around −78.01, −85.51, and −93.33 ppm (Figure 7b). The central peak at −85.51 ppm is ascribed to Q^2-linked tetrahedral Si in the bulk structure unambiguously. The existence of two extra side peaks and their intensities relative to the central peak indicates that the linkage of Si tetrahedra is modified significantly in the K-doped materials. The peak around −93.33 ppm can be assigned to the Q^3 signal, corresponding to the structure unit of a SiO_4 tetrahedron with three bridging oxide ions, indicative of linkage of Si_3O_9 rings with SiO_4 tetrahedra. The peak around chemical shift −78.01 ppm locates within the range for Q^1-linked tetrahedral Si such as the terminal tetrahedron of a tetrahedral chain, implying that the 3-fold ring is broken. The terminal tetrahedra may be stabilized by forming bonds with the oxygen atoms of the absorbed lattice water molecules. The dehydrated $Sr_{0.7}K_{0.3}SiO_{2.85}$ only shows the Q^2 and a broad and enhanced Q^3-linked tetrahedral Si peaks with the Q^1-linked tetrahedral Si peak at −78.01 ppm disappeared (Figure 7c), confirming that this Q^1-linked tetrahedral Si peak arises from the hydration. The as-prepared NPD $Sr_{0.7}K_{0.3}SiO_{2.85}$ sample shows a very similar spectroscopy with that of the dehydrated sample, implying no or a small amount of water in this sample. The TGA data (Figure 6) on the NPD $Sr_{0.7}K_{0.3}SiO_{2.85}$ showed that the sample still contains a small amount of water (∼2.5 wt %), only half of which are crystal lattice water that are lost after about 100 °C. This indicates that such a small amount of water has negligible effect on the ^{29}Si NMR signal of $Sr_{0.7}K_{0.3}SiO_{2.85}$.

DISCUSSION

The ^{29}Si NMR results for the $Sr_{0.7}K_{0.3}SiO_{2.85}$ materials provide insight into the local defect structures arising from the K-doping and lattice water molecules in $SrSriO_3$-based oxide ion conductors. The acceptor-doping of potassium in $SrSiO_3$ introduces the oxygen vacancies in the Si_3O_9 tetrahedral rings, and this may break the rings into Si_3O_8 chains, as revealed by the existence of Q^1-linked Si signal. The Si_3O_8 chain contains two three-coordinate terminal Si centers; at low temperature and with inclusion of water molecules, the oxygen atoms in the absorbed lattice water molecules can fill the vacancies in the Si_3O_8 chain, thus stabilizing the terminal Si (Figure 8a). This gave rise to a Q^1-linked ^{29}Si signal and transformed the Si_3O_8 chain into a Si_3O_{10} chain (Figure 8a), maintaining the four-coordinate geometry for the two terminal Si centers. Upon dehydration, the Q^1 signal disappeared and the Q^3 signal intensity increased in the dehydrated samples, revealing that the Si_3O_8 tetrahedral chains are not stable without the water oxygen bonding to the terminal Si (i.e., the three-coordinate Si in the Si_3O_8 chain is not stable) and implying they formed a linkage with two neighboring Si_3O_9 rings, leading to a Si_9O_{26} unit (Figure 8b), giving rise to the Q^3-linked tetrahedral Si centers. At high temperature and without inclusion of water molecules, the Si_3O_8 chains induced from the breaking of the $Si_3O_{9-\delta}$ rings may stretch out to link two neighboring Si_3O_9 rings to form the Si_9O_{26} unit (Figure 8b) straightforwardly.

In the tetrahedral layers along the *c*-axis of the $SrSiO_3$ structure, each Si_3O_9 ring is surrounded by another six rings in the same tetrahedral layer; the shortest inter-Si_3O_9 Si−Si distance is ∼4.7 Å (Figure 1b), and the shortest intertetrahedral-layer Si−Si distance along the *c*-axis is ∼5.1 Å (Figure 1a). These inter-ring Si−Si distances are significantly longer than the regular oxygen-bridged Si−Si distances (3.0 Å to 3.4 Å).[30−33] This makes it hard to condense the neighboring $Si_3O_{9-\delta}$ rings via sharing corners to accommodate the oxygen vacancies without opening the rings. Condensation of Si_3O_9 rings has been observed in $Rb_{14}Si_{10}O_{17}$,[34] which contains dimeric cyclotrisilicate anion $[Si_6O_{17}]^{10-}$. In the $SrSiO_3$ structure, the condensation of $Si_3O_{9-\delta}$ rings requires locally translating two neighboring $Si_3O_{9-\delta}$ units by at least 0.7 Å toward each other to shorten the inter-ring Si−Si distance to a reasonable value (e.g., 3.3 Å), which is, however, energetically unfavorable. Therefore, the breaking of the rings might be necessary for formation of the Q^3-linked tetrahedral Si centers to accommodate the oxygen vacancies in the K-doped $SrSiO_3$.

The TGA data of the hydrated $Sr_{0.7}K_{0.3}SiO_{2.85}$ show the material lost ∼7% water upon heating before 100 °C in a much quicker rate than that for the remaining loss of ∼3.5% water in the high-temperature region above 100 °C. This implies that most of the absorbed water molecules could be located in the grain surface and that at least one-third of the absorbed water molecules could enter into the lattice. Therefore, the hydrated $Sr_{0.7}K_{0.3}SiO_{2.85}$ sample may be formulated as $Sr_{0.7}K_{0.3}SiO_{2.85}\cdot\sim 1/3H_2O$, and this lattice water content is roughly equal to twice the oxygen vacancy content created by the K-doping in the hydrated $Sr_{0.7}K_{0.3}SiO_{2.85}$, which is sufficient to stabilize all the Si_3O_8 tetrahedral chains given that one oxygen vacancy breaks one Si_3O_9 ring and requires two water

dx.doi.org/10.1021/ic500891j | Inorg. Chem. 2014, 53, 6962−6968

molecules to bond with both terminal Si in the Si_3O_8 tetrahedral chain. The existence of Q^3-linked Si centers in the hydrated $Sr_{0.7}K_{0.3}SiO_{2.85}$ suggests that not all of the oxygen vacancies are filled by the oxygen atoms in the water molecules.

Although the ^{29}Si NMR data clearly show that the tetrahedral Si linkage is modified significantly in the K-doped $SrSiO_3$, it is hard to model such extended defect structure using the neutron diffraction data that relies on a periodic arrangement of atoms. No apparent residual nuclear scattering density peaks can be discerned from the difference Fourier map calculation. The vacancy preference on the bridging oxygen sites over the terminal oxygen sites from the structure refinement is consistent with the breaking of Si_3O_9 rings. Generally, modeling the local extended defect structures using the diffraction data remains a challenge in most of the materials as the diffraction technique probes the average structure. Such challenge has been encountered on the interstitial oxide ion conducting apatite, where the defects are extremely difficult to locate precisely, and the local distortion around the defect is hard to model using the neutron diffraction data.[7,9,35−40] Modeling the local defect structure in the apatite materials[12] relies on the advanced computational methods such as density functional theory (DFT) and molecular dynamic simulation, which is not in the scope of this study. The great contrast between the defect structure and average structure observed in the $Sr_{0.7}K_{0.3}SiO_{2.85}$ case in this study emphasizes the prominent capability of solid-state NMR in probing the local defect structure. This ring-breaking mechanism in K-doped $SrSiO_3$ revealed here might be applicable to Na-doped $SrSiO_3$, which was recently found to demonstrate the full potential to be electrolytes for commercial intermediate-temperature SOFCs given its highest low-temperature oxide ion conductivity and competitive cost among the chemically stable oxide ion conductors.[41]

4. CONCLUSION

In summary, the ^{29}Si NMR spectra of the $Sr_{0.7}K_{0.3}SiO_{2.85}$ samples revealed complex defect structures arising from the oxygen vacancies, in great contrast to the average structure of stabilizing oxygen vacancies within the isolated tetrahedral Si_3O_9 rings probed by the NPD data. The existence of Q^1-linked Si signal indicates breaking of the Si_3O_9 rings into Si_3O_8 chains, which are stabilized by bonding with the oxygen atoms in the absorbed water molecules or linking with the neighboring Si_3O_9 rings, forming Q^3-linked tetrahedral Si in the rings.

■ ASSOCIATED CONTENT

Supporting Information

Crystallographic data in CIF file of $Sr_{0.7}K_{0.3}SiO_{2.85}$. This material is available free of charge via the Internet at http://pubs.acs.org.

■ AUTHOR INFORMATION

Corresponding Authors

*E-mail: kuangxj@glut.edu.cn. (X.K.)
*E-mail: ceswmm@mail.sysu.edu.cn. (M.W.)

Notes

The authors declare no competing financial interest.

■ ACKNOWLEDGMENTS

This work is funded by National Science Foundation of China (No. 21101174), the Research Project (No. 213030A) of Chinese Ministry of Education, and Program for New Century Excellent Talents in University (No. NCET-13-0752). Thanks are also given to Guilin University of Technology and Chinese Ministry of Education Scientific Research Foundation for Returned Scholars for the Start-up Funds.

■ REFERENCES

(1) Kishimoto, M.; Iwai, H.; Miyawaki, K.; Saito, M.; Yoshida, H. *J. Power Sources* **2013**, *223*, 268−276.
(2) Thomas, C. I.; Kuang, X.; Deng, Z.; Niu, H.; Claridge, J. B.; Rosseinsky, M. J. *Chem. Mater.* **2010**, *22*, 2510−2516.
(3) Orera, A.; Slater, P. R. *Chem. Mater.* **2010**, *22*, 675−690.
(4) Li, M.; Pietrowski, M. J.; De Souza, R. A.; Zhang, H.; Reaney, I. M.; Cook, S. N.; Kilner, J. A.; Sinclair, D. C. *Nat. Mater.* **2014**, *13*, 31−35.
(5) Evans, I. R.; Howard, J. A.; Evans, J. S. *Chem. Mater.* **2005**, *17*, 4074−4077.
(6) Lacorre, P.; Goutenoire, F.; Bohnke, O.; Retoux, R.; Laligant, Y. *Nature* **2000**, *404*, 856−858.
(7) Ali, R.; Yashima, M.; Matsushita, Y.; Yoshioka, H.; Ohoyama, K.; Izumi, F. *Chem. Mater.* **2008**, *20*, 5203−5208.
(8) Kuang, X.; Green, M. A.; Niu, H.; Zajdel, P.; Dickinson, C.; Claridge, J. B.; Jantsky, L.; Rosseinsky, M. J. *Nat. Mater.* **2008**, *7*, 498−504.
(9) Kendrick, E.; Islam, M. S.; Slater, P. R. *J. Mater. Chem.* **2007**, *17*, 3104−3011.
(10) Esaka, T.; Mina-ai, T.; Iwahara, H. *Solid State Ionics* **1992**, *57*, 319−325.
(11) Packer, R. J.; Skinner, S. J. *Adv. Mater.* **2010**, *22*, 1613−1616.
(12) Panchmatia, P. M.; Orera, A.; Rees, G. J.; Smith, M. E.; Hanna, J. V.; Slater, P. R.; Islam, M. S. *Angew. Chem.* **2011**, *123*, 9500−9505.
(13) Li, M. R.; Kuang, X.; Chong, S. Y.; Xu, Z.; Thomas, C. I.; Niu, H.; Claridge, J. B.; Rosseinsky, M. J. *Angew. Chem., Int. Ed.* **2010**, *49*, 2362−2366.
(14) Kendrick, E.; Kendrick, J.; Knight, K. S.; Islam, M. S.; Slater, P. R. *Nat. Mater.* **2007**, *6*, 871−875.
(15) Singh, P.; Goodenough, J. B. *J. Am. Chem. Soc.* **2013**, *135*, 10149−10154.
(16) Singh, P.; Goodenough, J. B. *Energy Environ. Sci.* **2012**, *5*, 9626−9631.
(17) Martinez-Coronado, R.; Singh, P.; Alonso-Alonso, J.; Goodenough, J. B. *J. Mater. Chem. A* **2014**, *2*, 4355−4360.
(18) Ferrara, C.; Tealdi, C.; Pedone, A.; Menziani, M. C.; Rossini, A. J.; Pintacuda, G.; Mustarelli, P. *J. Phys. Chem. C* **2013**, *117*, 23451−23458.
(19) Sansom, J. E.; Tolchard, J. R.; Islam, M. S.; Apperley, D.; Slater, P. R. *J. Mater. Chem.* **2006**, *16*, 1410−1413.
(20) Holmes, L.; Peng, L.; Heinmaa, I.; O'Dell, L. A.; Smith, M. E.; Vannier, R.-N.; Grey, C. P. *Chem. Mater.* **2008**, *20*, 3638−3648.
(21) Lippmaa, E.; Mägi, M.; Samoson, A.; Engelhardt, G.; Grimmer, A. *J. Am. Chem. Soc.* **1980**, *102*, 4889−4893.
(22) Lippmaa, E.; Mägi, M.; Samoson, A.; Tarmak, M.; Engelhardt, G. *J. Am. Chem. Soc.* **1981**, *103*, 4992−4996.
(23) Lippmaa, E.; Mägi, M.; Tarmak, M.; Wieker, W.; Grimmer, A. *Cem. Concr. Res.* **1982**, *12*, 597−602.
(24) Smith, J. V.; Blackwell, C. S. *Nature* **1983**, *303*, 223−225.
(25) Magi, M.; Lippmaa, E.; Samoson, A.; Engelhardt, G.; Grimmer, A. *J. Phys. Chem.* **1984**, *88*, 1518−1522.
(26) Maekawa, H.; Maekawa, T.; Kawamura, K.; Yokokawa, T. *J. Non-Cryst. Solids* **1991**, *127*, 53−64.
(27) Martinez-Coronado, R.; Singh, P.; Alonso-Alonso, J.; Goodenough, J. B. *J. Mater. Chem. A* **2014**, *2*, 4355−4360.
(28) Coelho, A. *Topas Academic,* Version 4.1; Coelho Software: Brisbane, Australia, 2007.
(29) Nishi, F. *Acta Crystallogr., Sect. C* **1997**, *53*, 534−536.

(30) Moore, P. B.; Louisnathan, S. J. *Z. Kristallogr.* **1969**, *130*, 438−448.
(31) Tornroos, K. W. *Acta Crystallogr., Sect. C* **1994**, *50*, 1646−1648.
(32) Cruickshank, D.; Lynton, H.; Barclay, G. *Acta Crystallogr.* **1962**, *15*, 491−498.
(33) Yamnova, N.; Sarp, K.; Egorov-Tismenko, Y. K.; Pushcharovski, D.; Dasgupta, G. *Crystallogr. Rep.* **1993**, *38*, 464−467.
(34) Hoffmann, S.; Fässler, T. F. *Inorg. Chem.* **2006**, *45*, 7968−7972.
(35) Tolchard, J. R.; Islam, M. S.; Slater, P. R. *J. Mater. Chem.* **2003**, *13*, 1956−1961.
(36) Jones, A.; Slater, P. R.; Islam, M. S. *Chem. Mater.* **2008**, *20*, 5055−5060.
(37) Malavasi, L.; Orera, A.; Slater, P. R.; Panchmatia, P. M.; Islam, M. S.; Siewenie, J. *Chem. Commun.* **2011**, *47*, 250−252.
(38) Kendrick, E.; Orera, A.; Slater, P. R. *J. Mater. Chem.* **2009**, *19*, 7955−7958.
(39) Béchade, E.; Masson, O.; Iwata, T.; Julien, I.; Fukuda, K.; Thomas, P.; Champion, E. *Chem. Mater.* **2009**, *21*, 2508−2517.
(40) Panchmatia, P. M.; Orera, A.; Kendrick, E.; Hanna, J. V.; Smith, M. E.; Slater, P.; Islam, M. *J. Mater. Chem.* **2010**, *20*, 2766−2772.
(41) Wei, T.; Singh, P.; Gong, Y.; Goodenough, J. B.; Huang, Y.; Huang, K. *Energy Environ. Sci.* **2014**, *7*, 1680−1684.